


Comparison of Ultrasonographic Images of Glioblastoma Tumor with Magnetic Resonance Images: Rat Animal Model

Akram Shahidani¹, Manijhe Mokhtari- Dizaji^{1*} , Zeinab Shankayi², Mahmoud Najafi³

¹ Department of Medical Physics, Faculty of Medical Sciences, Tarbiat Modares University, Tehran, Iran

² School of Medicine, Baqiyatallah University, Tehran, Iran

³ Faculty of Mathematical Sciences, Kent State University, Ohio, USA

*Corresponding Author: Manijhe Mokhtari Dizaji
Email: mokhtarm@modares.ac.ir

Received: 13 October 2022 / Accepted: 02 January 2023

Abstract

Purpose: Magnetic Resonance Imaging (MRI) can guide the surgical strategy to identify brain tumors and monitor treatment response. It is possible to use transcranial Ultrasound (US) for periodical follow-ups. Ultrasound waves pass through the delicate areas of the skull called acoustic windows. In this study, the efficiency of ultrasound imaging was performed to diagnose glioblastoma brain tumors and the results were compared with MR images.

Materials and Methods: Male Wistar rats were anesthetized by intraperitoneal injection of Ketamine and Xylazine. A stereotaxic device was used to determine the injection coordinates. C6 GBM cell lines were injected into the brains of rats. After two weeks, the formation of a glioblastoma tumor was confirmed histopathologically. The brain of animals was imaged by B-mode ultrasound and MRI. The section with the largest tumor dimensions was selected and the dimensions of the skull and tumor were measured based on the pixel size of each of the imaging methods. Pearson coefficient of correlation and Limits Of Agreement (LOA) were calculated for comparisons of the skull and tumor dimensions.

Results: The skull and the tumor dimensions showed a significant correlation between the B-mode ultrasound and the MRI measurements ($R = 0.99$ and $p < 0.05$). According to the Bland-Altman analysis, the mean difference was 0.31 mm (SD = 0.20) for skull and tumor dimensions. The exact shape of the tumor is not completely clear in the ultrasound images, but it can be useful to detect the presence of the tumor and its approximate dimensions.

Conclusion: In conclusion, a glioblastoma tumor was produced in the male Wistar rat. The tumor dimensions were properly assessed by B-mode ultrasound image processing and compared with MR imaging.

Keywords: Ultrasonography; Magnetic Resonance Imaging; T2 Weighted; Glioblastoma Multiform Tumor.

1. Introduction

Magnetic Resonance Imaging (MRI) is essential for characterizing brain tumors. It guides the surgical strategy and is necessary to monitor treatment response [1]. However, MRI has several downsides such as time, transport, tolerance, availability, and high cost [2-4]. In contrast to MRI, transcranial ultrasound is a fast, non-invasive, well-tolerated, and low-cost method and can be done at the bedside [5-7]. Sonography is a first-line diagnostic technique that can reveal anatomical contours and show biological functions in in-vivo models [8]. It is possible to use transcranial ultrasound for periodical follow-ups. In addition to causing little stress to the patient, this type of imaging is cost-effective and can be monitored. Ultrasound imaging in the brain is complicated due to the presence of the skull in the way of ultrasound waves reaching the brain. The ultrasound waves are attenuated and deflected by the skull, especially in higher frequencies [9]. For this reason, transcranial ultrasound is usually performed through "acoustic windows" in the skull. Acoustic windows are areas where bone thickness is minimal and relatively uniform, such as the temporal and suboccipital windows [10-12]. In a study that investigated acoustic windows for photoacoustic imaging of intracranial blood vessels, it was shown that sphenoid sinus and ophthalmic acoustic windows provide images with the best target visibility and clarity [13]. Over the years, to investigate the impact of the skull on transcranial-focused ultrasound, researchers have done many works, including mapping the skull geometry [14], exploring the cranial acoustic parameters [15,16], cranial phantom experiment [17], and investigating the effect of skull thickness and density on transcranial focused ultrasound [18-20].

In experimental adult animal models, the skull causes low sensitivity, aberrations in the images, and loss of spatial resolution in ultrasound studies of the brain [21]. For this reason, studies have used not only specific ultrasound, such as photoacoustic and high-frequency ultrasound and functional ultrasound [21-23]. Investigators have also performed skull-thinning surgical procedures [23, 25] or removal of the skull of animals [26] for high-quality images. However, some authors reported that craniotomy can induce morphological and vascular changes in the rat brain [23]. Furthermore, blood flow can be studied with Doppler ultrasonography [21, 24], but a more complete study of the brain vasculature

in animal models is necessary with this technique. Biomedical implants or devices are introduced into the brain or skull using ultrasonography, while this is not possible with MRI [26]. Brain tumors can be detected between 40% and 80% by conventional transcranial ultrasound. The percentage of diagnosis depends on the type of tumor and the quality of the acoustic window [27].

Glioblastoma is one of the most aggressive and difficult cancers to treat. Patient life expectancy after diagnosis is only 12 to 18 months and 5-year survival is less than 10% [28]. Frutos *et al.* used a 13 MHz high-frequency transducer to identify brain structures in the rat. The probe was placed directly on the skin of the animal, then in front of the skull, through a limited craniotomy, and finally through a complete craniotomy. The results of this study showed that ultrasound images enable the identification of cerebral ventricles and subarachnoid cisterns, as well as the analysis of real-time monitoring of cerebral blood flow in the main arteries of the rat brain [29]. In this study, we have focused on imaging of rats using high-resolution ultrasound as a more accessible technique compared to MRI. This approach enables us to identify the internal dimensions of the skull and glioblastoma tumor and, the efficiency of ultrasound imaging was performed to diagnose glioblastoma brain tumors and the results were compared with MR images.

2. Materials and Methods

2.1. Ethics Statement

The experiments were carried out at the Tarbiat Modares university Laboratory, Tehran, Iran. Animal care and experimental procedures were designed to minimize animal suffering in compliance with and approved by the "Tarbiat Modares University Ethical Committee for Animal Research" (Code: IR.MODARES.REC.1399.137).

2.2. Animals

Male Wistar rats (2–3 months old, weighing 200-300 g) were used to compare MR and US images. They were kept under standard animal house conditions (22–23°C, 12–12 light-dark cycle, tap water, and standard laboratory diet). All experiments were performed in accordance with the ARRIVE guidelines [30]. During the tumor

induction and imaging session, the rats were anesthetized [31] with a mix of Ketamine (80 mg/kg) and Xylazine (8 mg/kg).

2.3. Tumor Induction

The animals were anesthetized by intraperitoneal injection of Ketamine and Xylazine. A stereotaxic device was used to keep the animal's head steady and determine the injection coordinates. With a Hamilton syringe, 10 microliter suspension consisting of 1 million C6 GBM cell lines (C6 glioblastoma cells) was injected into the brains of rats at the coordinates of 2 mm Anterior-Posterior (AP), 2 mm Right to Left (RL), and 4 mm Dorsal-Ventral (DV) relative to the bregma point [32]. Figure 1 shows the location of tumor induction and different regions of the skull. The steps of tumor induction are shown in Figure 2.

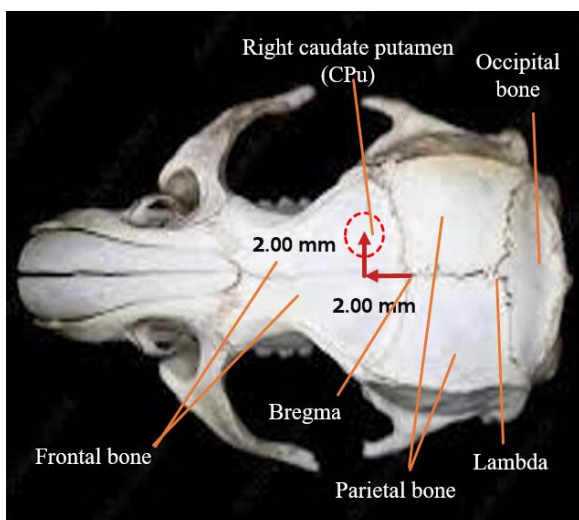


Figure 1. The location of tumor induction in caudate putamen (CPU) is indicated by the dashed circle

At the end of two weeks, the rats were sacrificed with the veterinarian injected a standard dose of the anesthetic ketamine and xylazine. After the rat was anesthetized, a high dose was injected for heart failure and death. The brain of rat was quickly removed from the sacrificed animal and washed in PBS. The pieces were fixed in 10% buffered formalin and embedded in paraffin. To characterize the general architecture of the brain, 4 mm thick cross sections were cut and mounted on glass slides and then stained with Hematoxylin-Eosin (H&E) for light microscopy and digital image acquisition (Olympus, BX51, Tokyo, Japan, magnification 3200). Histological studies were performed to confirm the formation of a glioblastoma tumor (Figure 3).

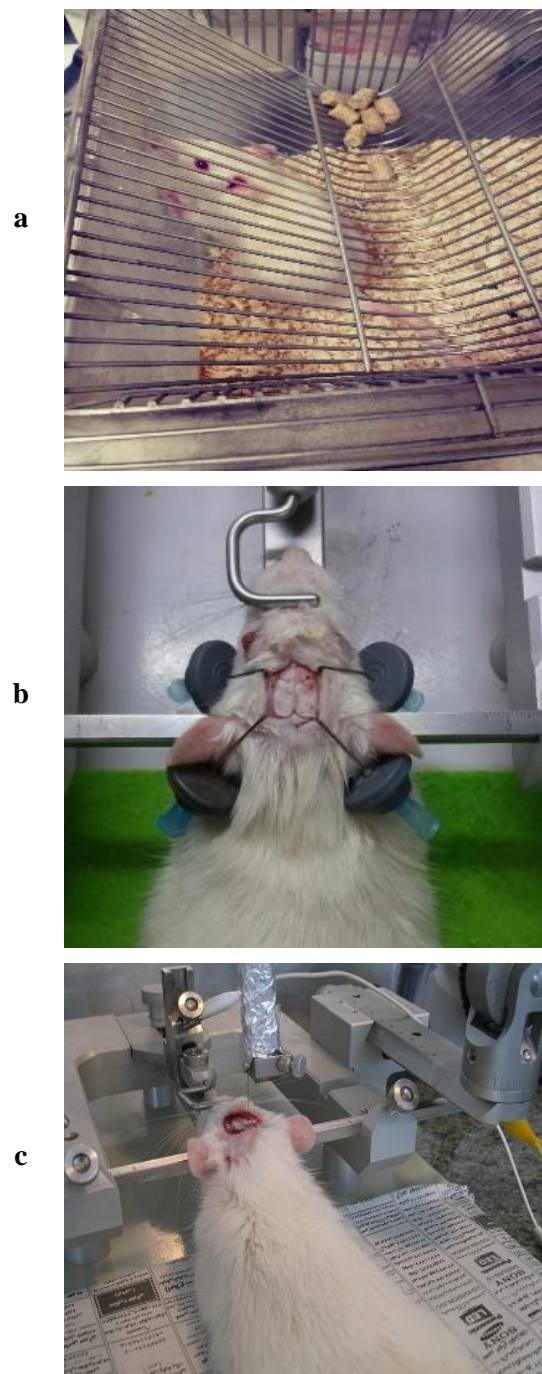


Figure 2. Tumor induction. a) Rat in a cage. b) A stereotaxic machine. c) A hamilton syringe to inject C6 glioblastoma cells

2.4. Sonography and MR Imaging

Brain images were acquired by transcranial MR imaging and sonography imaging. To obtain the MR images, the animals were anesthetized and a 3-Tesla Siemens Magnetom Prisma scanner and an animal head coil with a holder in the Iranian National Brain Mapping Laboratory (NBML) were used and images were taken with T2 weighted settings from the coronal direction.

MRI sections were perused. The section with the largest tumor dimensions was selected. For ultrasound images, on the same day, the animals were anesthetized. The hair on their heads was shaved and they were placed in a prone position. Then the brain and tumor were imaged using high-resolution ultrasound (Sonix Touch ultrasound system, Ultrasonix Medical Corporation, Richmond, Canada) at Tarbiat Modares University with probe settings at a 14 MHz frequency, 13 fr/s, and a 3 cm depth. In ultrasound, a scan was performed on the entire skull and the position with the largest tumor size was selected. The images were transferred to RadiAnt DICOM Viewer software (Medixant, Poznań, Poland) and the dimensions (the longitudinal and transverse of the skull and tumor) were extracted (n = 3) based on the pixel size of each of the imaging methods.

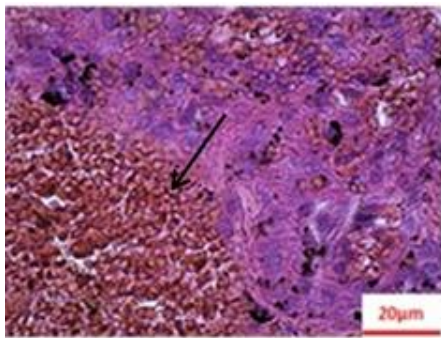


Figure 3. The result of histology after two weeks (Undifferentiated high grade)

2.5. Statistical Analysis

The results of the dimensions of the skull and tumor are presented as mean ± Standard Deviation (SD). The normality of dimensions was analyzed with the Kolmogorov–Smirnov test. To analyze the differences between the images, an independent t-test analysis was used with a level of significance of 0.05 ($p < 0.05$). The Pearson correlation coefficient (R) and linear regression functions between the results of ultrasound and MR examinations were analyzed with a p-value < 0.05 . The agreement between the B-mode ultrasound and MR measurements was analyzed using Bland-Altman analysis [33]. All data were analyzed using the SPSS software (SPSS/PC Inc., Chicago, IL).

3. Results

In the MR images, the skull and the tumor sizes were measured in the longitudinal and transverse directions with the maximum dimensions (Figures 4a and 4b).

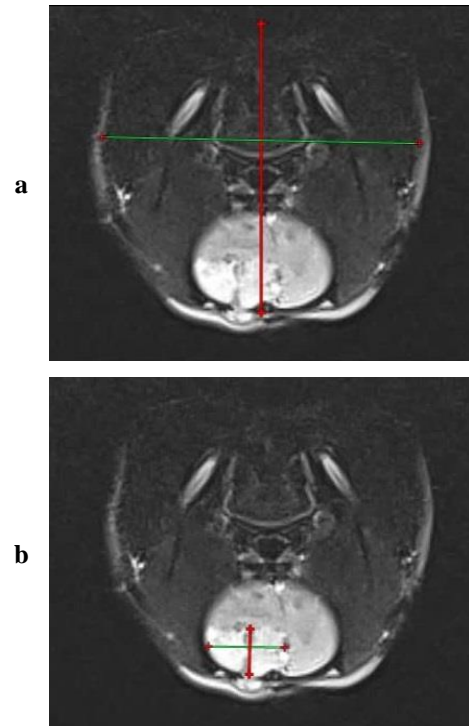


Figure 4. MR images of rat skull. a) Internal dimensions of the skull. b) Tumor dimensions

In the ultrasound images, the size of the rat skull and the tumor were measured in the longitudinal and transverse directions with the maximum cross-sectional area (Figures 5a and 5b).

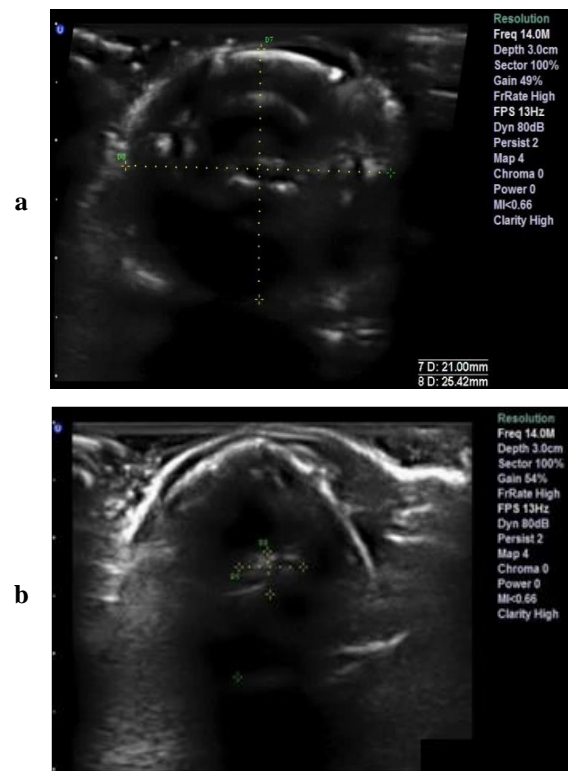


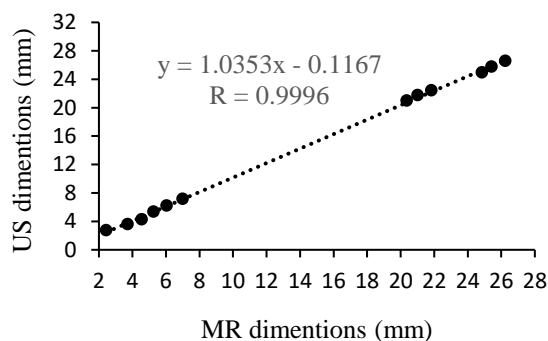
Figure 5. Ultrasound images of the rat's skull. a) Internal dimensions of the skull. b) Tumor's dimensions

Table 1. The mean±SD of the longitudinal and transverse size of the skull and the tumor with the two imaging methods (Ultrasonography and MRI)

Tissue	Skull		Tumor	
Direction	Length	Width	Length	Width
MRI	25.74 ± 0.65	21.69 ± 0.59	6.23 ± 0.74	3.52 ± 0.62
Ultrasonography	25.50 ± 0.57	21.06 ± 0.60	6.10 ± 0.72	3.57 ± 0.88
P-value	0.711	0.348	0.863	0.958

The results are shown in Table 1. There is no significant difference between the two imaging methods based on the longitudinal and transverse sizes of the skull and the longitudinal and transverse size of the tumor with independent t-test analysis ($P > 0.05$).

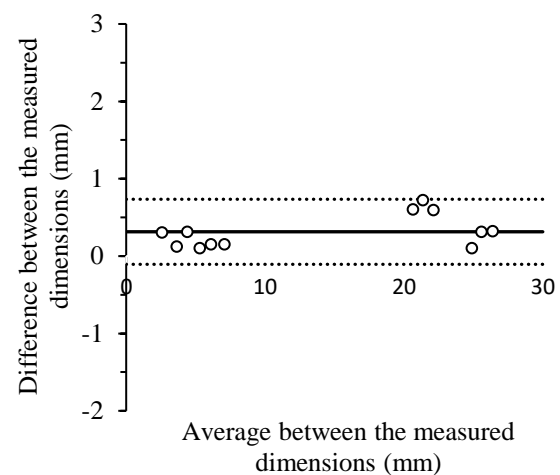
In this study, the relationship between the measured dimensions by ultrasound imaging and MR imaging methods was compared. The correlation between the sizes of the two methods was performed by Pearson correlation analysis. There was a high correlation between the skull and tumor dimensions by the two imaging methods ($R = 0.999$, $p < 0.05$) (Figure 6).

**Figure 6.** Scatter plots demonstrating the correlation between length and width (mm) of the skull and tumor measured with the ultrasonography method and MRI method

Using linear regression analysis, regression functions between the measured dimensions by ultrasonography (Y) and MRI (X) methods were calculated ($Y = 1.0353X - 0.1167$). The measured dimensions by the ultrasonography method were significantly correlated with the MRI method ($P < 0.05$).

For Bland-Altman analysis, the difference between the skull and the tumor sizes measured by the two imaging methods was plotted against the average of both measures. The middle line indicates the average difference between the two methods, whereas the outer lines represent 2SD

or the 95% Limits Of Agreement (LOA) (Figure 7). The confidence interval was 95%. There was a high agreement between the two methods. The mean difference between the two imaging methods was 0.314 mm.

**Figure 7.** Relative Bland-Altman plot of the difference between dimensions based on the ultrasound method and MRI method. The outer lines represent 1.96SD or 95% LOA

4. Discussion

The results of this study confirm that the measurements made based on ultrasound images have a significant correlation with the measurements from MR images. MRI is known as the gold-standard imaging technique to follow up on brain lesions, however, it also has some disadvantages, including limited accessibility, contrast-related side effects, and high costs [34]. The use of conventional ultrasound opens a new path of possibilities in the experimental research of neurological diseases in visualizing brain structures, as well as for monitoring cerebral blood flow. Ultrasound has several major advantages, including fast imaging speed, safety, and portability without the need for shielding as is required in MRI [4]. In addition, ultrasound can be used when there

is a metallic state, but it still has limitations. The human skull and the reflection of ultrasound waves are the most important challenges that limit brain ultrasonography. Using the orbit and delicate areas of the skull (known as an acoustic window) is a new technique that addresses these problems but has challenges in beamforming and ultrasound image formation. In previous studies, the blood flow through the skin has been monitored by ultrasonography. In these studies, the anterior cerebral artery has been determined from the temporal and occipital points of the brain [21, 29]. In another study using ultrasonography, the main vessels in the rat were described. Also an atlas of the main structures of the brain was obtained. This technique can be used in animal models of different neurological diseases [29]. Mehrad *et al.*'s [35] measurements obtained from ultrasound images have been compared with measurements obtained from the histopathologic method. Swanson *et al.* [36] compared the measurements of intrinsic foot muscle from the ultrasound and MR images. They showed that ultrasonography can be a valid and reliable alternative to MR in this field. It was found that ultrasound imaging detects vasculitic changes in large arteries more than contrast-enhanced imaging. Ultrasonography of cranial vessels is similar to MRI [37]. Akbari *et al.* [38] compared 3D ultrasound imaging of the total volume of the kidney with MRA imaging (reference standard). This method is time-consuming and not easily accessible. The total volume of the kidney is a biomarker and a reliable prognosis for autosomal dominant polycystic kidney disease. They found that 3D ultrasonography provides a promising technology for measuring kidney volume.

Some other studies have compared dimensions in the brain. Silva *et al.* [39] investigated the measurement of the brain and ventricle dimensions by inducing hydrocephalus using transcranial sonography. There was a significant correlation between transcranial ultrasonography and post-mortem samples for brain diameter ($R = 0.95$) and ventricle width ($R = 0.97$). Frutos *et al.* [40] performed in-vivo monitoring of Intracerebral Hemorrhage (ICH) volume and brain structure displacement in a rat animal model with B-mode ultrasound. In this study, imaging was done with MRI and B-mode ultrasound. The images of these two techniques showed a significant correlation in measuring the intracerebral hemorrhage volume. A significant correlation was observed in the measured distance between the subarachnoid and dura mater between B-mode ultrasound and MRI ($R = 0.870$). In our study,

correlation analysis shows a 0.999 coefficient of correlation between the skull and tumor dimensions in ultrasound images compared to MR images. A comparison of the values of B-mode ultrasonography and MRI methods showed a high correlation between the two methods ($R = 0.999$). Bland-Altman analysis was used to evaluate the estimated difference between the skull and tumor dimensions based on the B-mode ultrasonography and MRI methods. There was a high agreement between the two methods. In human applications, investigations should be done on beamforming and ultrasound formation, which was not our goal in this study.

5. Conclusion

This study is a preliminary evaluation to increase the efficiency of ultrasonography. Compared with MRI, our results show that ultrasonography provides relatively accurate measurements of the skull and glioblastoma tumor dimensions, and there is a high correlation between them. Since ultrasonography is more accessible than MRI, it can be effective in screening and follow-up treatments.

Acknowledgments

This study was approved by the Faculty of Medical Sciences, Tarbiat Modares University. This work was supported in part by the Iran National Science Foundation (INSF). MR images were acquired in the Iranian National Brain Mapping Laboratory (NBML).

References

- 1- Thust, S.C. *et al.*, "Glioma imaging in Europe: a survey of 2centersres and recommendations for best clinical practice." *European radiology*, Vol. 28 (No. 8), pp. 3306-3317 (2018).
- 2- Hemphill, J.C. *et al.*, "Guidelines for the management of spontaneous intracerebral hemorrhage: a guideline for healthcare professionals from the American heart Association/American stroke association." *Stroke*, Vol. 46 (No. 7), pp. 2032–2060 (2015).
- 3- Dastur, C.K. *et al.*, "Current management of spontaneous intracerebral hemorrhage." *Stroke and Vascular Neurology*, Vol. 2 (No. 1), pp. 21–29 (2017).
- 4- Lin, J.B. *et al.*, "Imaging of small animal peripheral artery disease models: recent advancements and

- translational potential." *International Journal of Molecular Sciences*, Vol. 16 (No. 5), pp. 11131–11177 (2015).
- 5- Meyer-Wiethe, K. et al., "Diagnosis of intracerebral hemorrhage with transcranial ultrasound." *Cerebrovascular Diseases*, Vol. 27 (No. 2), pp. 40–47 (2009).
 - 6- Blanco, P. et al., "Intracranial hematoma and midline shift detected by transcranial color-coded duplex sonography." *The American Journal of Emergency Medicine*, Vol. 33 (No. 11), pp. 1715.e5-1715.e7 (2015).
 - 7- Greco, A. et al., "Ultrasound biomicroscopy in small animal research: applications in molecular and preclinical imaging." *Journal of Biomedicine and Biotechnology*, Vol. 2012, pp. 1-14, (2012).
 - 8- Maresca, D. et al., "Biomolecular ultrasound and sonogenetics." *Annual Review of Chemical and Biomolecular Engineering*, Vol. 9, pp. 229–252 (2018).
 - 9- Fry, F.J. et al., "Acoustical properties of the human skull." *Journal of the Acoustical Society of America*, Vol. 63, pp. 1576–1590 (1978).
 - 10- Kirkham, F.J. et al., "Transcranial measurement of blood velocities in the basal cerebral arteries using pulsed Doppler ultrasound: velocity as an index of flow." *Ultrasound in Medicine and Biology*, Vol. 12, pp. 15–21 (1986).
 - 11- Smith, S.W. et al., "Feasibility study: Real-time 3-D ultrasound imaging of the brain." *Ultrasound in Medicine and Biology*, Vol. 30, pp. 1365–1371 (2004).
 - 12- Lindsey, B.D. et al., "Simultaneous bilateral real-time 3-D transcranial ultrasound imaging at 1 MHz through poor acoustic windows." *Ultrasound in Medicine and Biology*, Vol. 39, pp. 721–734 (2013).
 - 13- Graham Michelle T. et al., "Investigation of acoustic windows for photoacoustic imaging of intracranial blood vessels." In *2020 IEEE International Ultrasonics Symposium (IUS)*, pp. 1-4 (2020).
 - 14- Li, H. et al., "The Thickness Measurement of Alive Human Skull Based on CT Image." *Journal of Biomedical Engineering*, Vol. 24, pp. 964–968 (2007).
 - 15- Okita, K. et al., "The role of numerical simulation for the development of an advanced HIFU system." *Computational Applied Mechanics*, Vol. 54, pp. 1023-1033 (2014).
 - 16- Samoudi, M. et al., "Computational modeling of a single-element transcranial focused ultrasound transducer for subthalamic nucleus stimulation." *Neural Engineering*, Vol. 16, pp. 026015 (2019).
 - 17- Gatto, M. et al., "Three-Dimensional Printing (3DP) of neonatal head phantom for ultrasound: Thermocouple embedding and simulation of bone." *Medical Engineering and Physics*, Vol. 34, pp. 929–937 (2012).
 - 18- Saito, O. et al., "Substantial fluctuation of acoustic intensity transmittance through a bone-phantom plate and its equalization by modulation of ultrasound frequency." *Ultrasonics*, Vol. 59, pp. 94–101 (2015).
 - 19- Pichardo, S. et al., "Multi-frequency characterization of the speed of sound and attenuation coefficient for longitudinal transmission of freshly excised human skulls." *Physics in Medicine and Biology*, Vol. 56, pp. 219 (2011).
 - 20- Boutet, A. et al., "The relevance of skull density ratio in selecting candidates for transcranial MR-guided focused ultrasound." *Journal of Neurosurgery*, Vol. 132, pp. 1785–1791 (2020).
 - 21- Giustetto, P. et al., "Non-invasive parenchymal, vascular and metabolic high-frequency ultrasound and photoacoustic rat deep brain imaging." *Journal of Visualized Experiments*, Vol. 2015 (No. 97), pp. 4–5 (2015).
 - 22- Mac'E, E. et al., "Functional ultrasound imaging of the brain." *Nature Methods*, Vol. 8 (No. 8), pp. 662–664 (2011).
 - 23- Osmanski, B.F. et al., "Functional ultrasound imaging of intrinsic connectivity in the living rat brain with high spatiotemporal resolution." *Nature Communications*, Vol. 5 (No. 5023), pp. 1-14 (2014).
 - 24- Brunner, C. et al., "Mapping the dynamics of brain perfusion using functional ultrasound in a rat model of transient middle cerebral artery occlusion." *Journal of Cerebral Blood Flow and Metabolism*, Vol. 37 (No. 1), pp. 263-276 (2017).
 - 25- Mac' e, E. et al., "In vivo mapping of brain elasticity in small animals using shear wave imaging." *IEEE Transactions on Medical Imaging*, Vol. 30 (No. 3), pp. 550–558 (2011).
 - 26- Dill, T., "Contraindications to magnetic resonance imaging: non-invasive imaging." *Heart*, Vol. 94 (No. 7), pp. 943–948 (2008).
 - 27- Meyer, K. et al., "Transcranial sonography of brain tumors in the adult: an in vitro and in vivo study." *Journal of Neuroimaging*, Vol. 11 (No. 3), pp. 287-292 (2001).
 - 28- Alphandéry, Edouard. "Nano-therapies for glioblastoma treatment." *Cancers*, Vol. 12 (No. 1), pp. 242 (2020).
 - 29- Gomezmez-de Frutos, M.C. et al., "Identification of brain structures and blood vessels by conventional ultrasound in rats." *Journal of Neuroscience Methods*, Vol. 346, pp. 108935 (2020).
 - 30- Kilkenny, C. et al., "Improving bioscience research reporting: The ARRIVE guidelines for reporting animal research." *PLOS Biology*, Vol. 8, pp. 1000412 (2010).
 - 31- Heydarheydari, S. et al., "Pulsed high magnetic field-induced reversible blood-brain barrier permeability to enhance brain-targeted drug delivery."

- Electromagnetic Biology and Medicine*, Vol. 40 (No. 2), pp. 1-14 (2021).
- 32- Miura, F.K. *et al.*, "Experimental model of C6 brain tumors in athymic rats." *Arquivos de Neuro-Psiquiatria*, Vol. 66 (No. 2), pp. 238-241 (2008).
- 33- Moladoust, H. *et al.*, "Estimation of septal wall thickness by processing sequential echocardiographic images." *Iranian Cardiovascular Research Journal* Vol. 3, 24-33 (2009).
- 34- Morelli, L. *et al.*, "Role of abdominal ultrasound for the surveillance follow-up of pancreatic cystic neoplasms: a cost-effective safe alternative to the routine use of magnetic resonance imaging." *World Journal of Gastroenterology*, Vol. 25 (No. 18), pp. 2217–2228 (2019).
- 35- Mehrad, H. *et al.* "Ultrasonographic analysis versus histopathologic evaluation of carotid advanced atherosclerotic stenosis in an experimental rabbit model." *Ultrasound in Medicine and Biology*, Vol. 38, pp. 1391-1403 (2012).
- 36- Swanson, D.C. *et al.*, "Validity of ultrasound imaging for intrinsic foot muscle cross-sectional area measurements demonstrated by strong agreement with MRI." *BMC Musculoskeletal Disorders*, Vol. 23 (No. 1), pp. 1-12 (2022).
- 37- Yip, A. *et al.*, "Magnetic resonance imaging compared to ultrasonography in giant cell arteritis: a cross-sectional study." *Arthritis research and therapy*, Vol. 22 (No. 1), pp. 1-8 (2020).
- 38- Akbari, P. *et al.*, "Total Kidney Volume Measurements in ADPKD by 3D and Ellipsoid Ultrasound in Comparison with Magnetic Resonance Imaging." *Clinical Journal of the American Society of Nephrology*, Vol. 17 (No. 6), pp. 827-834 (2022).
- 39- Moura Silva, G.A.P. *et al.*, "Transcranial ultrasonography as a reliable instrument for the measurement of the cerebral ventricles in rats with experimental hydrocephalus: a pilot study." *Child's Nervous System*, Vol. 37, pp. 1863–1869 (2021).
- 40- Gomez -de Frutos M.C. *et al.*, "B-Mode Ultrasound, a Reliable Tool for Monitoring Experimental Intracerebral Hemorrhage." *Frontiers in Neurology*, Vol. 12, 771402 (2021).